Applied Catalysis B: Environmental 165 (2015) 306–315

Contents lists available at ScienceDirect

Applied Catalysis B: Environmental

journal homepage: www.elsevier.com/locate/apcatb

Gas phase oxidation of *n*-decane and PCE by photocatalysis using an annular photoreactor packed with a monolithic catalytic bed coated with P25 and PC500

Ricardo A.R. Monteiro[a], Sandra M. Miranda[a,b], Caio Rodrigues-Silva[a], Joaquim L. Faria[b], Adrián M.T. Silva[b,*], Rui A.R. Boaventura[a], Vítor J.P. Vilar[a,*]

[a] *LSRE – Laboratory of Separation and Reaction Engineering, Associate Laboratory LSRE/LCM, Faculdade de Engenharia, Universidade do Porto, Rua Dr. Roberto Frias, 4200-465 Porto, Portugal*

[b] *LCM – Laboratory of Catalysis and Materials, Associate Laboratory LSRE/LCM, Faculdade de Engenharia, Universidade do Porto, Rua Dr. Roberto Frias, 4200-465 Porto, Portugal*

ARTICLE INFO

Article history:
Received 18 August 2014
Received in revised form 9 October 2014
Accepted 10 October 2014
Available online 23 October 2014

Keywords:
Solar photocatalysis
Air decontamination
VOCs
TiO_2 PC500 and P25
Monolithic structures

ABSTRACT

Perchloroethylene (PCE) and *n*-decane are persistently present in the indoor air of several industrial/corporate facilities and households. The present paper reports studies on the photocatalytic oxidation (PCO) of *n*-decane and PCE using an annular photoreactor equipped with a compound parabolic collector (CPC) and packed with transparent cellulose acetate monolithic structures coated with two commercially available TiO_2, namely PC500 and P25, under simulated solar light. Such configuration allowed the illumination of the whole tubular reactor perimeter and catalytic bed, enhancing therefore the photonic efficiency and to take advantage of the low pressure drop and the high surface-area-to-volume ratio, typical of honeycomb reactors. The influence of the type of TiO_2, feed flow rate, pollutant concentration, relative humidity, gas-phase molecular oxygen and irradiance on the pollutants PCO was assessed. PC500 film showed higher conversion of both pollutants in comparison with P25 despite the lower mass of catalyst used for film coating. *n*-Decane ($C_{dec,feed}$ = 71 ppm) and PCE ($C_{PCE,feed}$ = 1095 ppm) conversions close to 100% were obtained operating at Q_{feed} = 150 cm^3 min^{-1} (τ = 88 s), I = 38.4 W_{UV} m^{-2} and RH = 40%. The mineralization's of PCE over both photocatalytic films were similar. However, *n*-decane was 100% and 69% mineralized respectively over PC500 and P25 films, under the same operating conditions. In addition, competitive adsorption between the pollutants and water molecules on the TiO_2 film surface was observed above 20% of RH. Results obtained at low RH suggest that $Cl^{\bullet}$ radical chain propagation reactions may be included in the PCO mechanism of PCE. Finally, the absence of oxygen drastically impairs the photoreaction.

1. Introduction

VOCs represent a very active group of air pollutants discharged into the atmosphere by household and industrial activities, such as fuel combustion, residential cleaning agents, among several others. For example, Teixeira et al. [1] reported a large concentration of VOCs, including perchloroethylene (PCE) and *n*-decane, in the indoor air of different stages of a wastewater treatment plant (WWTP), mainly associated with the aeration and mechanical agitation processes, as well as with the different sludge treatment stages. PCE, in particular, is widely used as model target pollutant due to its toxicity and carcinogenic potential to humans.

Since the pioneer work by Fujishima and Honda [2], the interest on photocatalytic processes applied to environmental issues has been growing every year, not only regarding photocatalytic processes (PCO) for water/wastewater treatment applications, but also for air purification [3–5]. The degradation of air pollutants by PCO is an attractive and efficient route when compared to other conventional techniques, such as adsorption on activated carbon, since the photocatalytic semiconductors are able to mineralize the pollutants, instead of a simple and more common phase transfer.

Several semiconductors are often employed as photocatalysts [6–11] and among them, TiO_2 (also known as titania) stands out as one of the most photoactive [12] under UV radiation. A number of commercial photocatalytic TiO_2 powders are available on the

* Corresponding authors. Tel.: +351 918257824; fax: +351 225081674.
E-mail addresses: adrian@fe.up.pt (A.M.T. Silva), vilar@fe.up.pt (V.J.P. Vilar).

http://dx.doi.org/10.1016/j.apcatb.2014.10.026
0926-3373/

market, being TiO_2 Aeroxide P25 from Evonik® the most commonly employed [13]. It is generally accepted that the high activity of P25 comes from the formation of heterojunctions between the two types of crystalline phases, anatase (80%) and rutile (20%), which may also explain the low activity of P25 under visible light in some particular cases [14]. Specifically, rutile, owing to its lower conduction band, may absorb some light in the visible range (red) and thus serve as a photosensitizer of the anatase phase. The respective positions and the difference between the higher energy levels of the conduction bands of the two phases may cause a transfer of electrons from anatase towards rutile, preventing at the same time charge recombination [15].

Although the actuating mechanism of pure anatase is well established, as regards P25 it has been over the years a matter of debate [16,17]. In a study conducted by Hajaghazadeh et al. [18], PC500 (consisting of 100% anatase) yielded a higher reaction rate than P25 in the degradation of gaseous methylethylketone under UVA light. The superior photocatalytic activity of PC500 was attributed to its higher specific surface area (SSA). Taranto et al. [19] also reported a slight higher photocatalytic activity of P25 over PC500 in the degradation of methanol and *n*-octane as gas-phase model pollutants. In another study conducted by Águia et al. [13], ten distinct commercially available photocatalysts were incorporated into a water-based exterior paint aiming NO photoabatement. The highest yields were obtained with the catalysts consisting of 100% anatase, such as PC500.

Reactor geometry is also a key factor in gas-phase photocatalysis due to its influence on optimizing the catalyst exposure to both radiation and reactants [20]. The most common photoreactors are tubular, annular and flat plate types [20–22]. Regarding the photocatalyst structural configuration, thin-film powder layer and/or fluidized bed [21,23], coated wall-parallel [24,25] and honeycomb/foam monolithic reactors [26–28] are probably the most representative.

This paper presents the results from a study on gas-phase solar photo-oxidation of two VOCs: *n*-decane and PCE. Two different commercially available TiO_2 photocatalysts (P25 from Evonik® and PC500 from Cristal®) were deposited onto the surface of a monolithic and transparent structure of cellulose acetate. Applying such structure into a annular reactor allows a high surface-area-to-volume ratio and a low pressure drop, typical of honeycomb reactors [29]. The photocatalytic efficiency of both photocatalytic films, using a continuous-flow annular photoreactor equipped with a compound parabolic collector (CPC), were compared. This configuration allows the illumination of the whole reactor perimeter and catalytic bed, enhancing therefore the photonic efficiency [30,31]. The PCO of *n*-decane and PCE over PC500 and P25 films were studied for different operating conditions, namely the feed flow rate (Q_{feed}), feed VOC concentration ($C_{dec,feed}$ or $C_{PCE,feed}$), and incident irradiance (I). The influence of relative humidity (RH), and the presence or absence of oxygen in the PCO of such compounds was also assessed using PC500 film. To the best of our knowledge, few papers have compared the efficiency of PC500 and P25 films in the gas-phase PCO of VOCs.

2. Experimental

2.1. Materials and methods

P25 and PC500 powders were supplied by Evonik® (formerly Degussa) and Cristal® (formerly Millennium), respectively, and used as delivered, without further modification or purification. Some characteristics of PC500 and P25 powders provided by the manufacturers are given in Table 1. Cellulose acetate monolithic structures (TIMax CA50-9/S – $L_C = 80$ mm, $d^2_{ch} = 9\,mm \times 9\,mm$, $e_{w,ch} = 0.1$ mm; Wacotech GmbH & Co. KG.) were used as substrate to affix the powders.*n*-Decane (≥94%; CAS no. 124-18-5; Merck), PCE (≥99.5%; CAS no. 127-18-4; Panreac Química S.A.U.) and deionized water were used for the generation of contaminated and humidified air streams. Helium N50 and nitrogen N50 (purity ≥99.999%), and synthetic air N50 (O_2: 20 ± 1%; H_2O: <3 ppm; C_nH_m: <0.1 ppm; CO_2: <1 ppm; CO: <1 ppm) were provided by Air Liquide.

Table 1
Catalysts, catalytic bed properties and dimensions of the photoreactor employed in the PCO of *n*-decane and PCE under simulated solar radiation.

TiO_2 catalysts		PCO of *n*-decane	PCO of PCE
PC500 (Cristal®)			
Crystal structure		>99% anatase	
Crystal size [nm]		5–10	
Surface area [$m^2\,g^{-1}$]		345	
E_g [eV]		3.3[a]	
m_{PC500} [mg]		52.3	35.3
$\rho_{A,PC500}$ [mg cm^{-2}]		6.48×10^{-2}	4.38×10^{-2}
P25 (Evonik®)			
Crystal structure		80% anatase, 20% rutile	
Crystal size [nm]		25	
Surface area [$m^2\,g^{-1}$]		50	
E_g [eV]		3.25[b]	
m_{P25} [mg]		74.7	100.4
$\rho_{A,P25}$ [mg cm^{-2}]		9.26×10^{-2}	1.24×10^{-1}
Photoreactor			
Outer tube (Pyrex-glass)	$d_{ot,e}$ [cm]		5.00
	$d_{ot,i}$ [cm]		4.64
Inner tube (quartz)	$d_{in,e}$ [cm]		2.00
	$d_{in,i}$ [cm]		1.64
Photoreactor	Length, L_R [cm]		16.0
	Volume, V_R [cm^3]		220

[a] Calculated by Ângelo et al. [63].
[b] Calculated in our previous work [64].

Monolithic cellulose acetate structures were evenly coated using aqueous suspensions of P25 and PC500 by the dip-coating method (Dip-Coater RDC21-K, Bungard Elektronik GmbH & Co. KG). Based on our previous work [32], nine layers of P25 or PC500 powder were deposited by immersing the monolithic structures on aqueous suspensions at a withdrawal rate of 0.8 mm s^{-1} assuring a thin and uniform film on each substrate surface (samples were dried at 323 K for 30 min between each layer deposition). Before coating, the monolithic structures were soaked for 1 h with distilled water and alkaline detergent (Derquim LM 01, Panreac Química, S.A.U.), subsequently washed with Milli-Q water, and dried at 323 K. The photocatalysts aqueous suspensions (2 wt.%) were sonicated for 10 min at 50 kHz in order to better disperse the particles.

The TiO_2-coated monolithic structures were assembled into the annular photocatalytic reactor (see Section 2.2) for the PCO study of *n*-decane and PCE. The catalytic bed properties are also detailed in Table 1.

2.2. Experimental setup and photocatalytic experiments

The schematic representation of the experimental setup is illustrated in Fig. 1 which is already carefully described in our previous work [33]. Briefly, humidified air stream contaminated with PCE or *n*-decane was generated by flowing air with 21% oxygen through different Woulff bottles (Normax, Lda.), one containing PCE or *n*-decane and another filled with deionized water (Fig. 1a). The flows were controlled by three mass flow controllers (MFC, El-Flow, Bronkhorst High-Tech B.V.). Oxygen-free experiments were performed by replacing the flowing air by nitrogen and removing dissolved oxygen in water by replacing deionized water by a

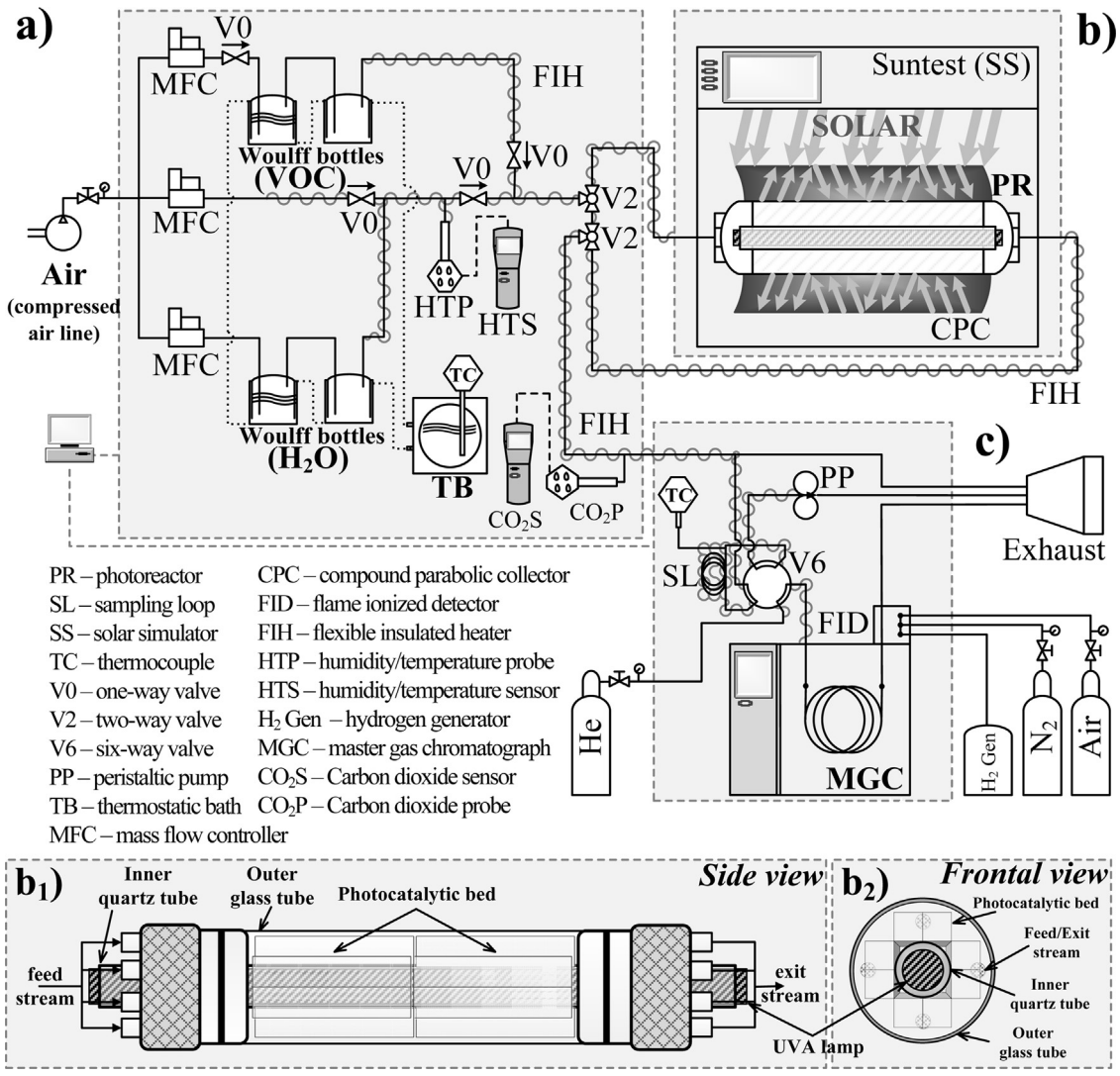

Fig. 1. Schematic representation of the experimental set-up and the continuous-flow photoreactor: (a) lab-scale unit used for the generation of air streams containing *n*-decane and water vapour; (b) sunlight simulator containing the photoreactor: (b_1) side view and (b_2) frontal view; (c) master gas chromatograph analytic system used for the analysis of the photoreactor feed and exit gas streams.

Adapted with permission from Lopes et al. [33]. Copyright © 2012, Elsevier.

$10\,g\,L^{-1}$ Na_2SO_3 solution in the Woulff bottle. The photocatalytic system entails three main parts (Fig. 1b): (i) a solar light simulator (Atlas, model Suntest XLS+) with $0.110\,m^2$ of working area illuminated by a 1700 W air-cooled Xenon arc lamp and an infrared coated quartz glass daylight filter reproducing the solar light spectrum within $300 < \lambda < 800$ nm; (ii) an electropolished anodized aluminium CPC with $0.023\,m^2$ of irradiated area able to use both direct and diffuse UV radiation [30,31]; (iii) an annular photoreactor (the outer tube made of soda-lime glass, Duran borosilicate glass 3.3, cut-off at 280 nm, Schott-Rorhglas GmbH; and the inner tube made of quartz, Quarzglas-Rohr Quarzglastechnik, GmbH & Co.). Table 1 summarizes the tube dimensions of the photoreactor and Fig. 1b_1 and b_2 schematically represent the side and frontal views of annular photoreactor, respectively. The feed and exit tubing are made of PTFE minimizing the adsorption of VOCs.

Gas-phase PCE and *n*-decane concentration histories were monitored using a gas chromatograph (MGC Fast GC, Dani Instruments S.p.A.) equipped with a flame ionization detector (FID) and a Volcol capillary column (20 m × 0.18 mm × 1.00 μm; Supelco, Sigma-Aldrich Co. LLC.), represented in Fig. 1c. The experimental setup was connected to a computer and controlled using a data acquisition board system and an in-house program developed routine written in Labview environment (NI Corporation). All connections are of 1/16 in. stainless steel tubing to reduce dead volumes. Additionally, the CO_2 concentration of the photoreactor feed/exit stream was monitored online using an Indoor Air IAQ-Calc™ quality meter 7545 (TSI, Inc.).

All experiments were carried out inside the chamber of the solar light simulator (Fig. 1b), being the incident irradiance measured by a broadband UV radiometer (CUV 5, Kipp & Zonen B.V.), placed outside the outer tube and at the same height, within a spectral range of 280–400 nm corresponding to the UV fraction of the solar radiation.

The efficiency of the PCO process of both TiO_2 photocatalytic films towards *n*-decane and PCE degradation were compared in similar operational conditions and calculated as follows:

$$\text{Conversion}\ (\%) = \left(1 - \frac{C_{VOC,exit}}{C_{VOC,feed}}\right) \times 100 \quad (1)$$

At steady-state, VOC photodegradation fractions ($C_{VOC,exit}/C_{VOC,feed}$, where $C_{VOC,feed}$ and $C_{VOC,exit}$ are the pollutant

concentration in the feed and exit gas streams, respectively, expressed in ppm) were studied for different experimental conditions: Q_{feed} (75–300 $cm^3\ min^{-1}$, measured at 1 bar and 298 K), $C_{VOC,feed}$ ($C_{dec,feed}$ = 71–283 ppm and $C_{PCE,feed}$ = 548–2738 ppm), *RH* of the feed gas stream both in the presence and absence of oxygen (3–40%, measured at 1 bar and 298 K), and *I* (18.9–38.4 $W_{UV}\ m^{-2}$, measured in the spectral range 280–400 nm: UV fraction of the incident sunlight).

The mineralization yield of *n*-decane and PCE due to PCO was also evaluated and calculated as follows:

$$\text{Mineralization}\,(\%) = \left(\frac{C_{CO_2,exit}}{C_{VOC,feed}} \times \frac{1}{n}\right) \times 100 \quad (2)$$

where *n* is the number of carbons present in each pollutant molecular structure and $C_{CO_2,exit}$ is the CO_2 exit stream concentration.

Before turning on the solar simulator, the catalytic bed was continuously fed and several exit stream samples were measured until reaching a constant VOC concentration. Finally, at steady state conditions, the VOC conversion was determined for each experiment.

3. Results and discussion

3.1. VOCs photolysis

Blank experiments (*i.e.* photoreactor without TiO_2-photocatalytic film) were performed under three different incident irradiances, *i.e.* 18.9, 29.1, and 38.4 $W_{UV}\ m^{-2}$ (reference values to the sunlight UV fraction on the 280–400 nm range) in order to establish the effect of direct photolysis on the conversion of *n*-decane and PCE. No degradation of *n*-decane or PCE was observed for the range of irradiances tested (data not shown).

3.2. Catalytic film performance

3.2.1. Influence of the feed flow rate and VOC concentration

Fig. 2 illustrates the effect of the feed flow rate (Q_{feed}) on the *n*-decane (Fig. 2a) and PCE (Fig. 2c) photocatalytic conversion over PC500 (full coloured columns) and P25 (columns with patterns) films. Increasing Q_{feed}, the conversion of *n*-decane and PCE reduced regardless the employed irradiance (*i.e.* 18.9, 29.1, and 38.4 $W_{UV}\ m^{-2}$) or the type of catalytic film. More than 99% of the initial *n*-decane ($C_{dec,feed}$ = 71 ppm) and PCE ($C_{PCE,feed}$ = 1095 ppm) were converted over PC500 under *I* = 38.4 $W\ m^{-2}$ when the feed flow rates of 75 $cm^3\ min^{-1}$ and 150 $cm^3\ min^{-1}$ were set; on the other hand, 93% and 86% of *n*-decane and 99% of PCE conversions were attained over P25 film for the same experimental conditions. Increasing Q_{feed} to 300 $cm^3\ min^{-1}$, *n*-decane conversion decreased to approximately 65 and 91% while PCE conversion decreased to 67% and 92%, respectively over P25 and PC500 films.

In order to better understand the extent of the catalytic film activity towards the conversion of *n*-decane and PCE, the effect of Q_{feed} on the pollutant photocatalytic reaction rate, r_{VOC}, was also assessed as shown in Fig. 2b and d, respectively. The upmost values of *n*-decane reaction rate over PC500 (full coloured columns) and P25 (columns with patterns) films – 1.64×10^{-5} mol min^{-1} and 1.17×10^{-5} mol min^{-1}, respectively – were attained when using the highest Q_{feed} (300 $cm^3\ min^{-1}$) under *I* = 38.4 $W\ m^{-2}$. Although the highest conversion was observed at Q_{feed} = 75 $cm^3\ min^{-1}$ and *I* = 38.4 $W\ m^{-2}$ (>99%), r_{dec} was the lowest (4.43×10^{-6} mol min^{-1} and 4.15×10^{-6} mol min^{-1} respectively over PC500 and P25 films). Similarly, Fig. 2d shows the PCE reaction rate, r_{PCE}, over PC500 and P25 films. As seen before for *n*-decane, higher Q_{feed} (300 $cm^3\ min^{-1}$) promoted higher PCE reaction rates (2.20×10^{-4} mol min^{-1} and 1.59×10^{-4} mol min^{-1} respectively over PC500 and P25 films) under *I* = 38.4 $W\ m^{-2}$. In opposition, setting the lowest Q_{feed} (75 $cm^3\ min^{-1}$) both TiO_2 photocatalytic films promoted the highest PCE conversions (99%) and the lowest PCE reaction rates for each employed irradiance.

In both cases, the results suggest a double antagonistic effect as the feed flow rate increases [34,35]: (i) a decrease in the residence time inside the reactor decreases the adsorption of the pollutant molecules on the photocatalytic film surface which impairs the efficiency of the PCO process; (ii) higher organic load entering the photoreactor will enhance the mass transfer between the pollutant molecules and the catalytic film surface resulting in higher PCO reaction rates.

Regarding the efficiency of both catalytic films, it is worth noting that P25 film provided lower values of photocatalytic reaction rate than PC500 film in the PCO of *n*-decane and PCE: *n*-decane reaction rate values over P25 film were 6 up to 41% lower than over PC500 film depending on irradiance and feed flow rate as well as, the differences between both catalytic films in terms of reaction rates become greater as the Q_{feed} increased and *I* decreased. For example, for Q_{feed} = 75 $cm^3\ min^{-1}$ the photocatalytic reaction rates of *n*-decane over P25 film were 6–13% lower than over PC500 film as *I* decreases from 38.4 to 18.9 $W\ m^{-2}$; for Q_{feed} = 300 $cm^3\ min^{-1}$ the reaction rates over P25 film were 29–41% lower for the reduction in *I*. The same trend was observed for the PCO of PCE: P25 film provided up to 34% lower PCE reaction rates than PC500 film, employing the above described experimental conditions.

Fig. 3 shows the influence of the feed concentration of *n*-decane ($C_{dec,feed}$) and PCE ($C_{PCE,feed}$) on their conversion and on the PCO reaction rate. For the same residence time inside the photoreactor (τ = 88 s; Q_{feed} = 150 $cm^3\ min^{-1}$) the conversion of *n*-decane (Fig. 3a) and PCE (Fig. 3c) decreased as the feed concentration increased, regardless the catalytic film used. Employing PC500 film more than 98% of *n*-decane conversion was attained for the three irradiances employed (*i.e.* 18.9, 29.1, and 38.4 $W_{UV}\ m^{-2}$) when $C_{dec,feed}$ = 71 ppm, whereas P25 film yielded 74 up to 86% conversion, depending on the irradiance (Fig. 4a). Also, increasing *n*-decane feed concentration ($C_{dec,feed}$ = 142 ppm) the conversion of *n*-decane over PC500 film decreased in the range of 5–25% for an irradiance reduction from 38.4 to 18.9 $W\ m^{-2}$; over P25 film the reduction was around 20–30% for the same irradiance reduction. It is interesting to note that, at this concentration and fixing Q_{feed} = 150 $cm^3\ min^{-1}$ and *RH* = 40%, the *n*-decane conversion over P25 film is closer to that found when the photoreactor was packed with PC500 film and fed with twice the *n*-decane feed concentration, *i.e.* 283 ppm. In particular, 50, 62 and 69% of *n*-decane ($C_{dec,feed}$ = 142 ppm) was converted over P25 film, while 37, 51 and 62% was converted over PC500 film ($C_{dec,feed}$ = 283 ppm) under 18.9, 29.1 and 38.4 $W_{UV}\ m^{-2}$.

The activity of both photocatalytic films towards PCE conversion as a function of the PCE feed concentration ($C_{PCE,feed}$) is shown in Fig. 4c. As seen before for *n*-decane conversion over P25 and PC500 films, PCE conversion follows the same trend, *i.e.* the efficiency of the process decreases as the PCE feed concentration increases. In the range of 549–2738 ppm of $C_{PCE,feed}$, a 42% reduction in the PCE conversion (from 99 to 57%) can be observed under *I* = 18.9 $W_{UV}\ m^{-2}$ (Fig. 4c). It is worth noting that under higher irradiance (38.4 $W_{UV}\ m^{-2}$) no efficiency loss was observed in the same PCE concentration range. Although P25 film promoted PCE conversions of approximately 99% (Q_{feed} = 150 $cm^3\ min^{-1}$, $C_{PCE,feed}$ = 1095 ppm and *RH* = 40%) under 38.4 $W_{UV}\ m^{-2}$, it is under lower irradiances that the differences between both catalytic film activities become greater: 87 and 75% of PCE conversion were attained under 29.1 and 18.9 $W_{UV}\ m^{-2}$ of irradiance over P25 film, while 98 and 97% were converted over PC500 film under the same operational conditions. Increasing the PCE feed concentration from 1095 ppm to 1643 ppm, the P25 film promoted 13, 27 and 56% less

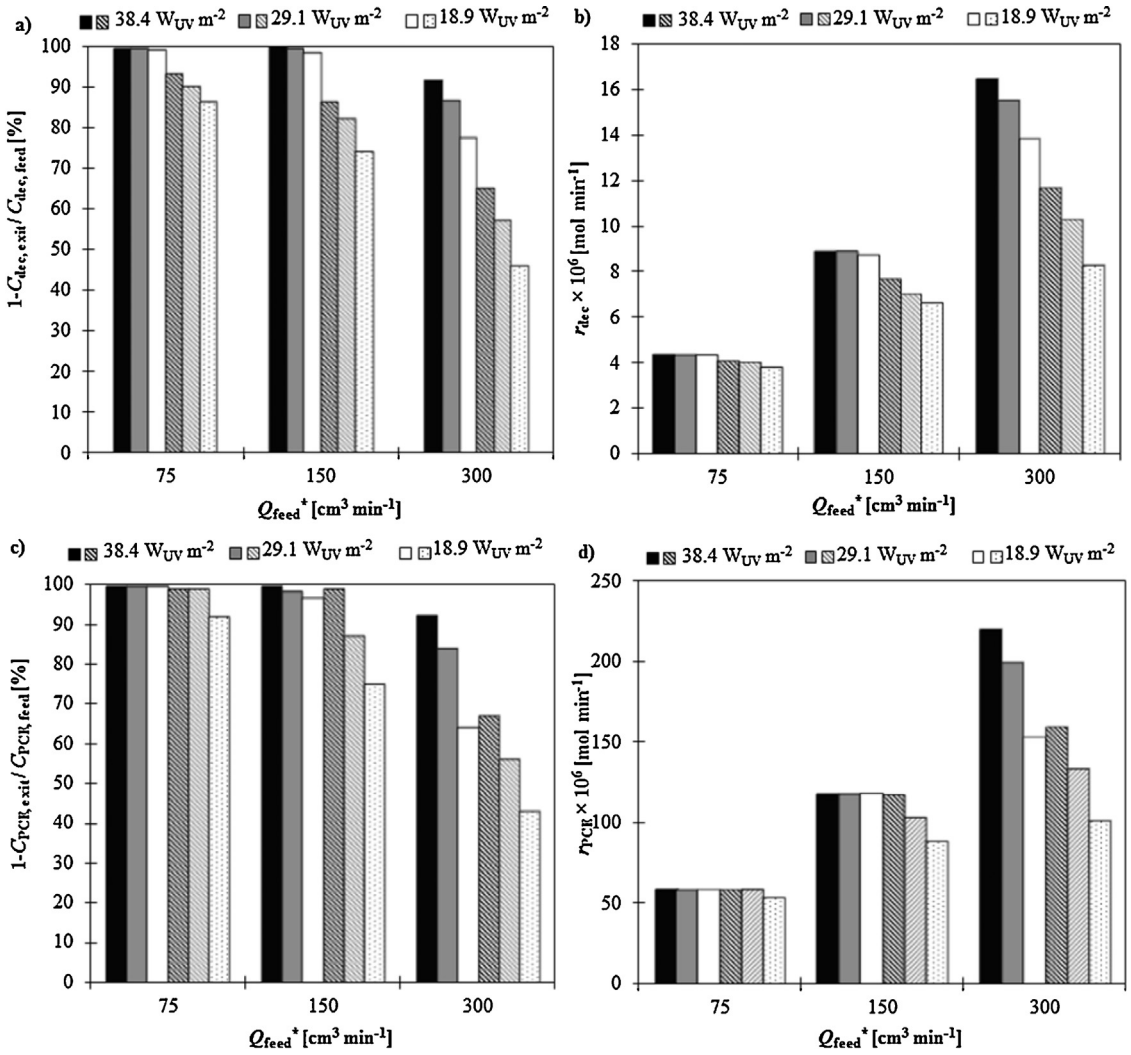

Fig. 2. Effect of feed flow rate [Q^*_{feed}] on the conversion of *n*-decane (a) and PCE (c) and on photocatalytic reaction rate, r_{VOC} ((b) and (d), respectively). Experimental points for incident irradiances of 38.4 W_{UV} m^{-2} (■,▨), 29.1 W_{UV} m^{-2} (■,▨), and 18.9 W_{UV} m^{-2} (□,⬚), measured within the spectral range of 280–400 nm, at steady-state conditions; $C_{dec,feed}$ = 71 ppm $C_{PCE,feed}$ = 1095 ppm, *RH** = 40% and 21% oxygen. Full coloured columns represent PC500 (■,■,□) and columns with patterns P25 (▨,▨,⬚) films. *Measured at 298 K and 1 bar.

PCE conversion than over PC500 respectively under 38.4, 29.1 and 18.9 W_{UV} m^{-2}.

A similar approach regarding the photocatalytic reaction rates of *n*-decane can be followed as plotted in Fig. 3b and d: under the three incident irradiances employed (38.4, 29.1 and 18.9 W_{UV} m^{-2}) and over PC500 and P25 films the reaction rate of *n*-decane and PCE increases as $C_{VOC,feed}$ increases. This means that, for the same flow rate, higher $C_{dec,feed}$ and $C_{PCE,feed}$ enhances the mass transfer between the feed gas stream and the catalyst surface and consequently the pollutants adsorption on the catalyst surface, increasing the amount of degraded pollutant.

For a given pollutant feed concentration and/or feed flow rate, the photocatalytic reaction rate depends on the number of oxidant species formed at the surface of the catalytic film. Likewise, the number of oxidant species depends on the photon flux. Hereupon, an increase in the irradiance is followed by an increase in the number of generated photons which will form an equivalent number of electro-hole pairs (and oxidant species) ultimately resulting in VOCs conversion gains. From Figs. 2 and 3 it is possible to see that the photocatalytic reaction rate of *n*-decane (Figs. 2b and 3b) and PCE (Figs. 2d and 3d) over PC500 and P25 films becomes more dependent on the incident irradiation as the organic load increases (higher Q_{feed} or $C_{VOC,feed}$): while for low organic loads the incident irradiance has almost no effect on the reaction rate of the VOC, for higher organic loads the reaction rate is nearly proportional to the irradiance employed, within the range 18.9–38.4 W_{UV} m^{-2}. This phenomenon is related to number of organic molecules entering the reactor and the number of photons available: at low organic loads the photons are in excess under the three irradiances, converting all or almost all available pollutant molecules; in opposition, at high organic loads the number of pollutant molecules to be converted is higher and the photons are no longer in excess requiring higher number of photons to achieve similar conversion values. This means that, higher organic loads make a better use of the photons regardless the efficiency loss of the PCO process.

The mineralization of *n*-decane and PCE over PC500 and P25 photocatalytic films is represented in Fig. 4. Although the mineralization of PCE over both photocatalytic films provided similar values for each irradiance (*ca.* 39, 31 and 24% under 38.4, 29.1 and 18.9 W_{UV} m^{-2}, respectively) the results show that PC500 film was able to yield higher mineralization of *n*-decane: 100% of *n*-decane ($C_{dec,feed}$ = 71 ppm) was mineralized into CO_2 and water whereas over P25 film only 69% of *n*-decane was mineralized under 38.4 W_{UV} m^{-2}. As expected, decreasing the irradiance so did the

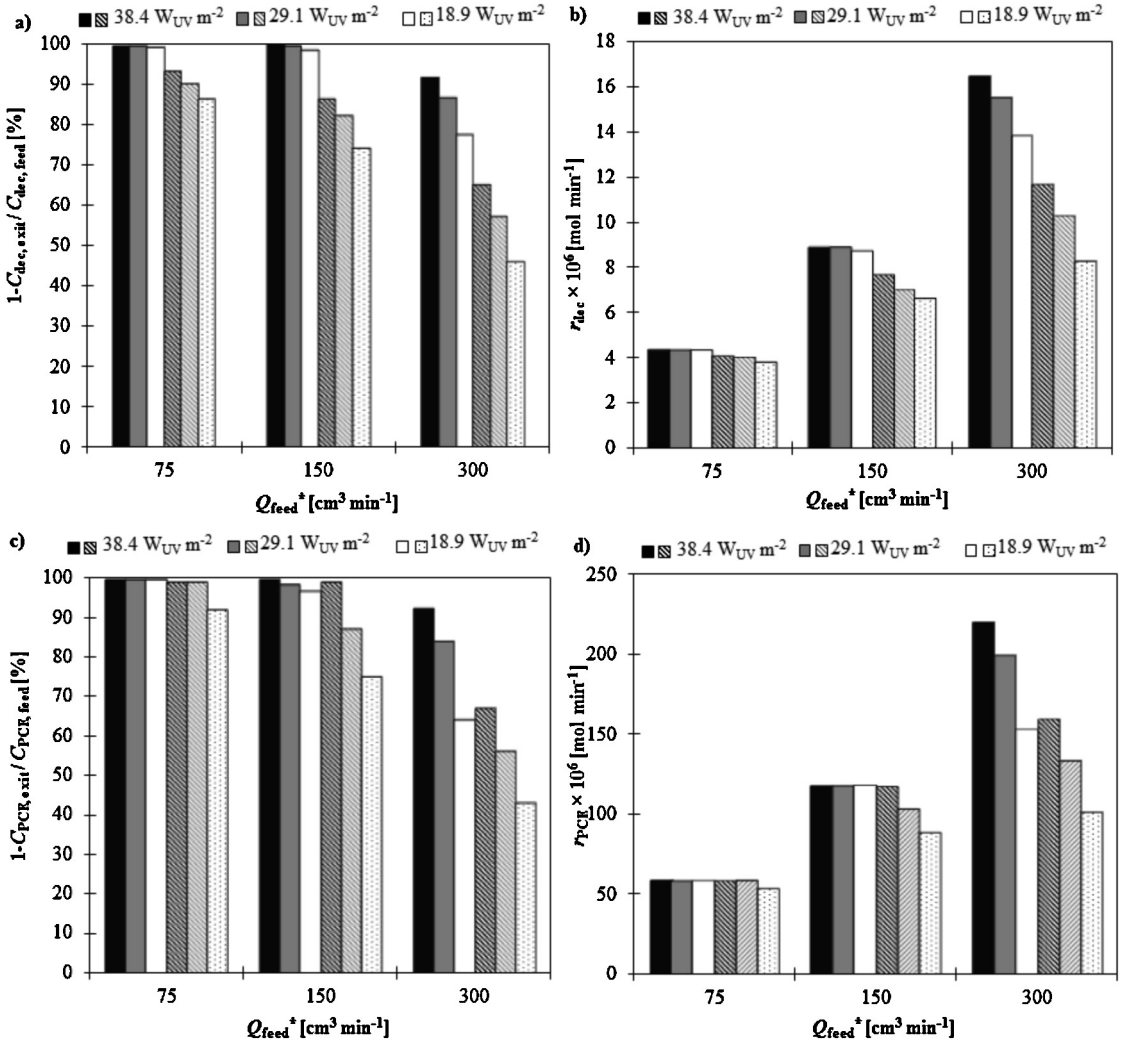

Fig. 3. Effect of VOC feed concentration ($C_{dec,feed}$, and $C_{PCE,feed}$) on the conversion of *n*-decane (a) and PCE (c) and on the photocatalytic reaction rate, r_{VOC} ((b) and (d), respectively). Experimental points for incident irradiances of 38.4 W_{UV} m^{-2} (■,▨), 29.1 W_{UV} m^{-2} (■,▨), and 18.9 W_{UV} m^{-2} (□,⊡) measured within the spectral range of 280–400 nm, at steady-state conditions; Q^*_{feed} = 150 cm^3 min^{-1}, *RH** = 40% and 21% oxygen. Full coloured columns represent PC500 (5) and columns with patterns P25 (▨,▨,⊡) films. *Measured at 298 K and 1 bar.

n-decane mineralization: under 29.1 and 18.9 W_{UV} m^{-2}, PC500 film was able to mineralize 83 and 73% while P25 film only mineralized 54 and 40%, respectively.

It should be pointed out that after more than 50 h under simulated solar radiation and continuous feed (humid air contaminated with *n*-decane or PCE), similar *n*-decane and PCE conversions (less than 1% of variation) were obtained under the same operating conditions and for both photocatalytic films (data not shown). Considering the results and our previous works where cellulose acetate monolithic structures were used as substrates [32,36,37], it is suggested that deterioration of the support and/or the photocatalytic film was negligible.

From this study, seems clear that PC500 film promotes higher conversions and higher reaction rates of *n*-decane and PCE than P25 film, under solar radiation, even considering that the produced PC500 film has lower mass of PC500 photocatalyst which may be an economic advantage. However, it is a challenging task to explain why PC500 film promoted higher photocatalytic conversions than P25 film in gas-phase experiments. For the last decades, several research works have been focused on the structure of P25 craving to understand the generally accepted superior activity of P25 over other commercially available photocatalysts mainly in liquid-phase studies [14,15,38–40]. Bickley et al. [15] attributed high photocatalytic activity of P25 to the presence of rutile and anatase phases. Admitting that each photocatalyst particle consists of an anatase core and a thin rutile cover layer, photogenerated holes of the anatase core would be effectively transferred to the rutile layer. However, Ohno et al. [38] stated that P25 powder consists, in fact, of relatively large rutile particles and very small anatase particles, which independently form agglomerates before mixing. They also stated that the superior activity of P25 was due to the proper band bending in rutile particles, which are in contact to anatase particles. Hurum et al. [14] concluded that the higher activity of mixed-phase TiO_2 was due to a more stable charge separation by electron transfer from rutile to lower energy anatase lattice trapping sites. On the other hand, Sun et al. [39] proposed that, in aqueous phase, the contact between anatase and rutile phases and a subsequently band bending between the two phases promotes a good charge-carrier separation. But such synergistic effect of anatase and rutile in aqueous phase is not exclusive to P25. Ohno et al. [40] reported the enhanced efficiency for mixed anatase and rutile at different ratios as well as thermally treated anatase yielding the two phases. It is worth noting that rutile phase can be formed in anatase samples by heat treatment [41] changing the crystallinity and the

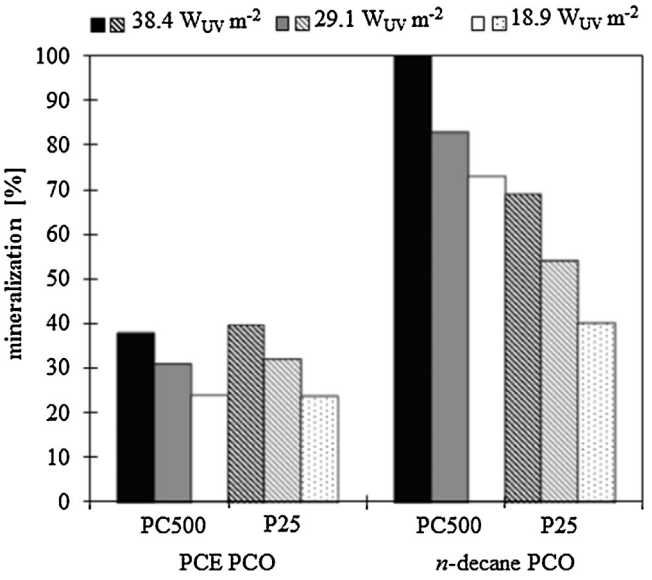

Fig. 4. Mineralization yields of PCE and *n*-decane due to PCO over PC500 and P25 films. Experimental points for incident irradiances of 38.4 W_{UV} m^{-2} (■,▨), 29.1 W_{UV} m^{-2} (■,▨), and 18.9 W_{UV} m^{-2} (□,⊡) measured within the spectral range of 280–400 nm, at steady-state conditions; $C^*_{PCE,feed}$ = 1095 ppm, $C^*_{dec,feed}$ = 71 ppm, Q^*_{feed} = 150 cm^3 min^{-1}, *RH** = 40% and 21% oxygen. Full coloured columns represent PC500 (■,■,□) and columns with patterns P25 (▨,▨,⊡) films. *Measured at 298 K and 1 bar.

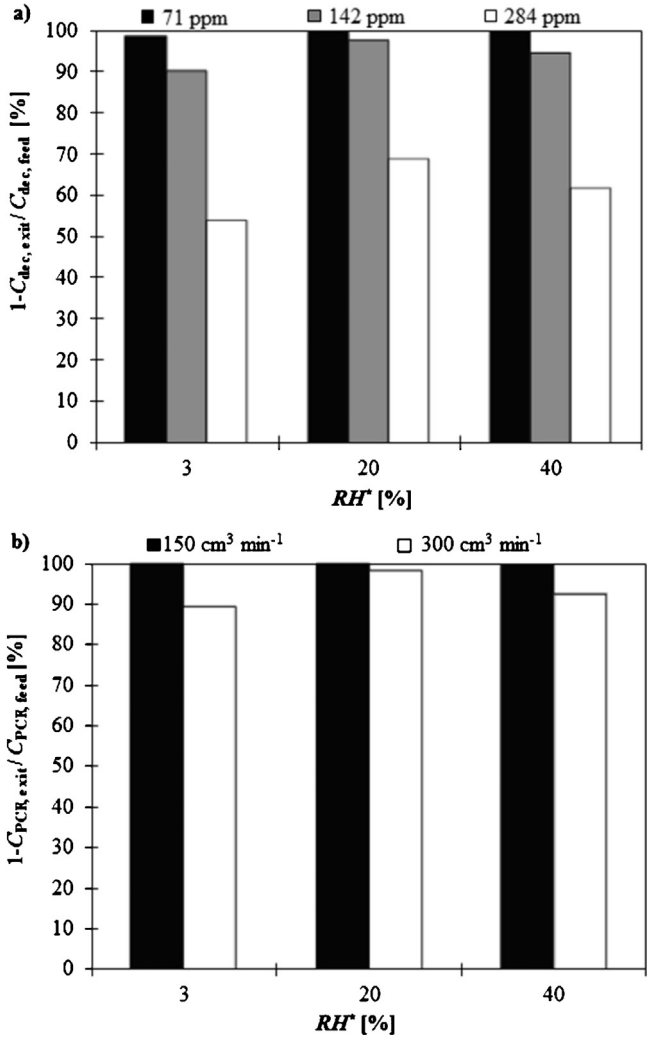

Fig. 5. Effect of water content [*RH**] on the conversion over PC500 film of: (a) *n*-decane, at steady-state conditions, for $C_{dec,feed}$ = 71 ppm (■), $C_{dec,feed}$ = 142 ppm (■), $C_{dec,feed}$ = 284 ppm (□), and Q_{feed} = 150 cm^3 min^{-1}; (b) PCE ($C_{PCE,feed}$ = 1095 ppm), at steady-state, for Q^*_{feed} = 150 cm^3 min^{-1} (■) and Q^*_{feed} = 300 cm^3 min^{-1} (□); 21% oxygen and I = 38.4 W_{UV} m^{-2}, measured within the spectral range of 280–400 nm. *Measured at 298 K and 1 bar.

size of TiO_2 particles which can affect the photocatalytic activity [14,42].

In gas-phase photocatalytic reactions, the contact between the two P25 phases may not be so effective and, thus, the synergistic effect may not be observed. An insufficient band bending will impair the contact between the two phases resulting in poor charge-carrier separation and, subsequently, in a loss of photocatalytic efficiency of mixed-phases TiO_2. In the absence of any synergistic effect between the anatase and rutile mixed TiO_2 phases, it is accepted that anatase is much more active than rutile in the PCO of organic compounds in water and air [43]. Even considering that the smaller crystal size of PC500 (Table 1) may foresee higher density in surface defects [19] reducing the electron–hole recombination time, which ultimately results in lower photocatalytic efficiencies, the larger surface area of PC500 in comparison to P25 which may be related to the higher adsorption capacity may justify the superior activity of PC500 [34,43,44].

3.2.2. Effect of the relative humidity on PCO of n-decane and PCE over PC500 film

The effect of the water content on the conversion of *n*-decane (Fig. 4a) and PCE (Fig. 4b) over PC500 film was evaluated for three *RH* conditions (3, 20, and 40%). Fig. 4a presents the conversion of *n*-decane attained under each *RH* condition for three given $C_{dec,feed}$. Fixing $C_{dec,feed}$ at 71 ppm (2.87×10^{-3} mol m^{-3}), a negligible decrease of 1.4% was observed as the water content decreases from 40 to 3% (3.61×10^{-1} mol m^{-3} to 2.71×10^{-2} mol m^{-3} of water; water/*n*-decane molar ratio of 125.8 and 9.4, respectively). The effect of *RH* on the *n*-decane conversion became clearer as the initial concentration of *n*-decane increases. Setting the *n*-decane feed concentration four times higher ($C_{dec,feed}$ = 284 ppm or 1.15×10^{-2} mol m^{-3}), it was observed that when *RH* was reduced from 20% (1.81×10^{-1} mol m^{-3} of water) to 3% the *n*-decane conversion also decreased (from 69 to 54%). The water/*n*-decane molar ratio is approximately 2.4 and 15.7 for *RH* of 3–20%. This indicates that water/*n*-decane molar ratios higher than 2.4 and lower than 9.4 are required to produce the necessary number of hydroxyl radicals for the pollutant degradation. On the other hand, at higher *RH* (40%) no improvement in the *n*-decane conversion was observed most likely due to competitive adsorption of *n*-decane and water molecules on the photocatalytic film surface. The same behaviour was observed for a $C_{dec,feed}$ = 142 ppm, but in this case, differences are less evident due to the high conversions of *n*-decane hiding the real effect of the water content variation.

Fig. 5b shows the effect of *RH* on the conversion of PCE over PC500 film, but instead of varying the feed concentration of the pollutant, two feed flow rates were tested (150 cm^3 min^{-1} and 300 cm^3 min^{-1}) for the same $C_{PCE,feed}$ (1095 ppm). For Q_{feed} = 150 cm^3 min^{-1}, no effect owed to the variation of *RH* was observed on the PCE conversion. However, doubling the total flow rate to 300 cm^3 min^{-1}, it becomes clear that *RH* has similar impact on the PCE conversion, in comparison with that described before for *n*-decane (Fig. 5a). The conversion of PCE reached its highest value (98%) when *RH* was set to 20%, while only 92 and 89% of the initial PCE were converted at 40 and 3% *RH*, respectively. It is important to note that at *RH* = 3% the concentration of water is lower than that of PCE ($C_{H2O,\ feed}$ = 2.71×10^{-2} mol m^{-3} and $C_{PCE,feed}$ = 4.43×10^{-2} mol m^{-3}) which would foresee a drastic

reduction of PCE conversion regardless Q_{feed}. However such reduction was not observed which may indicate further mechanisms in the photodegradation of PCE besides the classical attack of hydroxyl radicals. Chlorine radicals chain propagation reactions have been a matter of discussion by several research groups in an attempt to explain the PCO mechanism of chlorinated compounds [45–47].

The opposing effect of the water content has already been discussed in several research works and even so it still is a matter of debate [35,48–51]. Several authors reported that the absence of water vapour will seriously retard the conversion of several chemicals and their mineralization to CO_2 may become incomplete, but excessive water vapour may inhibit the degradation by competitive adsorption on the photocatalyst surface [48,52]. For instance, Obee and Brown [49] demonstrated that the oxidation rates of formaldehyde, toluene, and 1,3-butadiene (sub-ppmv concentrations) increase as the humidity decreases (for water content above *ca.* 1000 ppm). They suggested that the influence of humidity and trace contaminant concentrations on the oxidation rates on TiO_2 surface is due to the competitive adsorption on the available hydroxyl adsorption sites and to changes in hydroxyl radical population levels. The effect of water content on PCO of 1-butene (1.12×10^{-4} mol m^{-3}) over TiO_2 and SnO_2 was also investigated by Cao et al. [50]. These authors observed high photoactivity of SnO_2 at low water vapour contents (<1000 ppm or 4.09×10^{-2} mol m^{-3}) and a drastic reduction of photoactivity after increasing the water content above 2000 ppm (8.18×10^{-2} mol m^{-3}). TiO_2 films showed stable performance for water concentrations between 0 and 3000 ppm (1.12×10^{-1} mol m^{-3}). Pengyi et al. [35] showed that the photocatalytic conversion of trace toluene concentrations (4.09×10^{-5} to 8.18×10^{-4} mol m^{-3}) by O_3/UV, TiO_2/UV and O_3/TiO_2/UV processes was slightly affected by the relative humidity in the range 20–55% (2.04×10^{-1} to 7.77×10^{-1} mol m^{-3}) being the optimal humidity around 35% (4.82×10^{-1} mol m^{-3}). In a similar study, Zhang and Liu [53] reported that the relative humidity played a significant role in reducing trace hexane concentrations (5.73×10^{-5} to 3.12×10^{-4} mol m^{-3}) by TiO_2/UV and O_3/TiO_2/UV processes. The authors found that little humidity improved the decomposition of hexane whereas relative humidity above 45% (1.96×10^{-1} mol m^{-3}) would depress the decomposition. Jo and Park [51] revealed that photo-oxidation of benzene, ethyl benzene, and *o*-, *m*-, *p*-xylenes, trichloroethylene, and perchloroethylene in trace levels was independent of humidity in the range 10–100% (0.10–1.03 mol m^{-3}).

3.2.3. *Effect of oxygen on n-decane and PCE PCO over PC500 film*

The effect of the gas-phase molecular oxygen absence on the pollutants conversion over PC500 film under different *RH* conditions is depicted in Fig. 6 (columns with patterns). Fig. 6a shows a drastic reduction on the *n*-decane conversion after removing the oxygen feed gas stream from the reaction: only 16% of *n*-decane was converted at *RH* = 40% against more than 99% conversion when 21% of oxygen was present, under the highest irradiance used in this study (*I* = 38.4 W_{UV} m^{-2}). Reducing *RH* from 40 to 3% the conversion of *n*-decane decreased by 36%, *i.e.* from 16% to 10% under the same irradiance. Reducing irradiance to *I* = 29 W_{UV} m^{-2} *n*-decane conversion also reduced. For instance, 14% of *n*-decane was converted at *RH* = 40%, while only 1% of *n*-decane was converted at *RH* = 3%. For the lowest irradiance applied (*I* = 18.9 W_{UV} m^{-2}), no *n*-decane conversion was observed for both *RH* conditions in the absence of oxygen. A similar trend may be perceived from Fig. 6b, which represents PCE photocatalytic conversion experiments. Under 40% of *RH* the initial PCE was converted by 15 and 6% for *I* = 38.4 W_{UV} m^{-2} and *I* = 29.1 W_{UV} m^{-2}, respectively, whereas under 3% of *RH* no PCE conversion was detected. In addition, no PCE conversion was observed for *I* = 18.9 W_{UV} m^{-2} regardless the *RH* value in the gas stream.

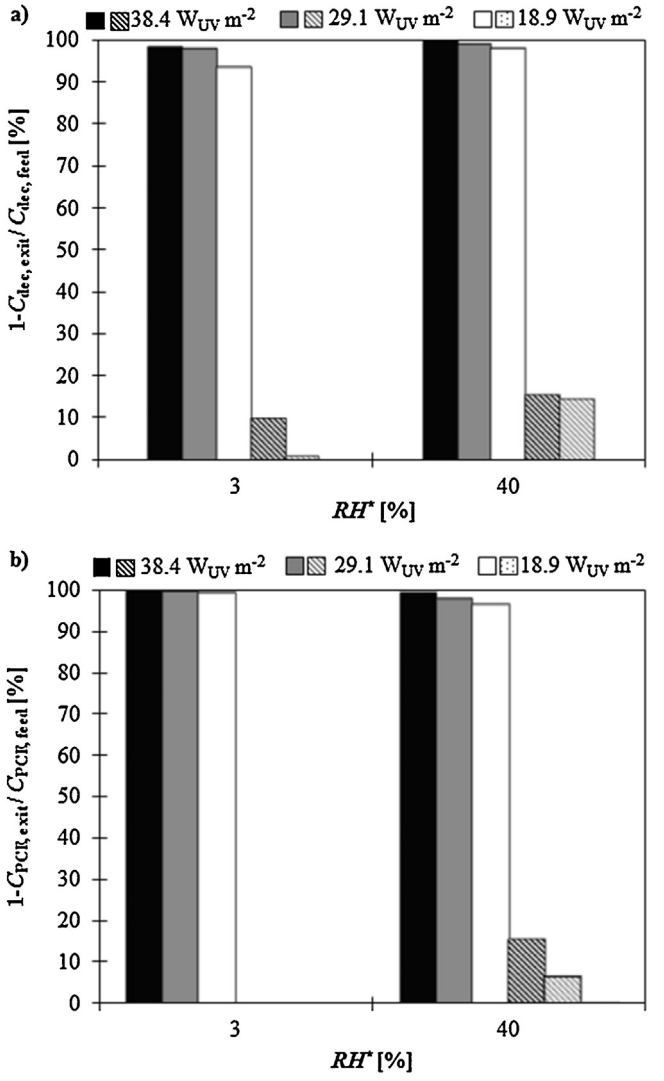

Fig. 6. Effect of water content [*RH**] on the conversion over PC500 film: (a) *n*-decane conversion at steady-state conditions for $C_{dec,feed}$ = 71 ppm; (b) PCE conversion at steady-state conditions for $C_{PCE,feed}$ = 1095 ppm. Full coloured columns (■,■,□) and columns with patterns (▨,▨,⬚) represent the presence of oxygen (21%) and its absence, respectively; Q^*_{feed} = 150 cm^3 min^{-1}, *I* of 38.4 W_{UV} m^{-2} (■,▨), 29.1 W_{UV} m^{-2} (■,▨) and 18.9 W_{UV} m^{-2} (□,⬚) were measured within the spectral range of 280–400 nm. *Measured at 298 K and 1 bar.

The presence of oxygen has been reported as essential for the photoreaction and increasing the oxygen concentration so does the pollutant decomposition rate [30,54–57]. Yet, the mechanism of action is not clear. Larson et al. [30] found that the complete oxidation of 2-propanol by UV/TiO_2 was dependent on the presence of oxygen: the conversion of acetone increased from 20 to 70% after 6 min of UV radiation as the oxygen content increased from 0% to 5% (v/v). They also observed that in the absence of gas-phase oxygen the photo-oxidation of propanol could still take place through TiO_2 lattice oxygen atoms and that oxygen was needed only to replenish the produced oxygen vacancies on the TiO_2 lattice. Muggli et al. [54–56] reported the photo-oxidation of acetic and formic acids over TiO_2 lattice oxygen and found that gas-phase oxygen replenishes the lattice oxygen vacancies even in the dark. On the other hand, they observed that when gas-phase oxygen was present the oxidation rate of formic acid was greatly improved, suggesting the important role of adsorbed oxygen. Likewise, El-Maazawi et al. [57] proposed that the photocatalytic reaction could take place in the

absence of oxygen due to the TiO_2 lattice oxygen. The oxygen from TiO_2 lattice is depleted during the conversion of gaseous acetone being replenished by the oxygen from the feed gas stream.

Considering that the conversion of the two pollutants (*n*-decane and PCE) was drastically hindered after removing the gas-phase molecular oxygen from the gas stream, two oxygen-related mechanisms may be involved in their photocatalytic conversion [30,54–57]. The first is based on the photodissociation of gas-phase molecular oxygen from the feed stream at the TiO_2 surface into O^-, which spontaneously reacts with O_2 forming O_3^-. These species may greatly contribute to the conversion of pollutants being at the same time the limiting step of the photocatalytic reaction. The second mechanism, where no gas-phase oxygen is present, may be related to the oxygen existing in the TiO_2 lattice. Assuming the limited availability of surface lattice oxygen, it would be expected that the photocatalysis would be considerably impaired, as it was, in fact, observed (see Fig. 6). Regardless of the presence or absence of gas-phase molecular oxygen and the surface density of TiO_2 on the substrate, it is possible to observe in both Figs. 5 and 6 that increasing the *RH* the conversion of the pollutants also increases as it was already previously discussed. The contribution of the classic photocatalytic mechanism where HO• radicals initiate the photocatalytic process certainly explain such behaviour. Another hypothesis for the role of HO• radicals is based on the ability of such species to act as effective traps for the holes preventing electron-hole recombination [58,59]. In this way the reduced titanium centres (produced by reductive reaction between $e^-_{CB}(TiO_2)$ and Ti^{4+} centre of the TiO_2) will enhance the space charge layer resulting in a longer lifetime, which ultimately promotes the oxidation of more gas-phase molecular oxygen [58,59].

Several authors have followed another meaningful approach to clarify the mechanism of PCE degradation by PCO [45–48,60–62]. However, agreement is yet to be found. On one hand, different authors [45–47] claimed that Cl• radical addition to PCE occurs several times faster than HO• radical addition, neglecting therefore the role of HO• radical. Such conclusion was further substantiated by Lu et al. [61] and Fan and Yates [62] after finding that the surface hydroxyl groups were inactive in the oxidation of methyl chloride and trichloroethylene. On the other hand, Yamazaki et al. [48,60], for example, stated that the PCO of PCE could occur *via* HO• radical or Cl• radical, but they concluded that Cl• radical initial reaction rarely occurs on the catalyst surface since the reaction with HO• radical is thermodynamically favourable.

4. Conclusions

Different photocatalytic oxidation (PCO) reactions under simulated solar radiation showed that films using the commercial TiO_2 photocatalyst PC500 provide higher conversions of PCE and *n*-decane than those obtained with standard P25. It was also found that PC500 film provides higher mineralization of *n*-decane than P25 film. Although the smaller crystallite size of P25 nanoparticles suggests the possibility of higher density in surface defects impairing the charge carriers and, therefore the PCO reaction, the higher surface area of PC500 catalyst may justify its superior performance towards the conversion of *n*-decane and PCE in comparison to P25 catalyst under steady state conditions.

Regarding PC500 film, it was evidenced the effect of the relative humidity (*RH*) on the photocatalytic conversion of both pollutants. The results suggest that for *RH* in the range 320%, the competitive adsorption between water and pollutant molecules is unlikely to occur, considering the pollutants concentration range studied. However, at 40% of *RH* the pollutant conversion over PC500 film decreases meaning competitive adsorption between the above-mentioned molecules. The conversion of *n*-decane and PCE by PCO was drastically impaired or even no observable in the absence of gas-phase molecular oxygen, which indicates the key role of oxygen in photocatalysis. Three major mechanisms may be implicit in the effect of the oxygen content. One is the formation of reactive species from the adsorbed gas-phase molecular oxygen, which will oxidize the pollutants. The second involves the action of the oxygen from the lattice of TiO_2. The third mechanism involves the classical HO• radical formation on the TiO_2 surface. Cl• radicals chain propagation reactions may also be involved in the PCO reaction mechanism of chlorinated compounds such as PCE.

Acknowledgements

Financial support for this work was mainly provided by the FCT (Fundação para a Ciência e a Tecnologia) project PTDC/EQU-EQU/100554/2008. This work was also supported by projects PEst-C/EQB/LA0020/2013 and PEst-OE/QUI/UI0616/2014, financed by FCT and FEDER through COMPETE, and by QREN, ON2 (North Portugal Regional Operational Programme) and FEDER through projects NORTE-07-0162-FEDER-000050, NORTE-07-0162-FEDER-000015. V.J.P.V. and A.M.T.S. acknowledge the FCT Investigator 2013 Programme (IF/00273/2013 and IF/01501/2013, respectively), with financing from the European Social Fund and the Human Potential Operational Programme. R.A.R.M. acknowledges FCT for his PhD (SFRH/BD/69323/2010) research fellowship and C.R-S. acknowledges CAPES for providing his Post-doctoral (8674/13-2) research scholarship, and the project CAPES/FCT 308/11 for financial support.

References

[1] J.V. Teixeira, S.M. Miranda, R.A.R. Monteiro, F.V.S. Lopes, J. Madureira, G.V. Silva, N. Pestana, E. Pinto, V.J.P. Vilar, R.A.R. Boaventura, Environ. Monit. Assess. 185 (2013) 59–72.
[2] A. Fujishima, K. Honda, Nature 238 (1972) 37–38.
[3] M.R. Hoffmann, S.T. Martin, W. Choi, D.W. Bahnemann, Chem. Rev. 95 (1995) 69–96.
[4] D.S. Bhatkhande, V.G. Pangarkar, A.A.C.M. Beenackers, J. Chem. Technol. Biotechnol. 77 (2002) 102–116.
[5] J.-M. Herrmann, Top. Catal. 34 (2005) 49–65.
[6] M. Anpo, Pure Appl. Chem. 72 (2000) 1787–1792.
[7] C.F. Lin, C.H. Wu, Z.N. Onn, J. Hazard. Mater. 154 (2008) 1033–1039.
[8] T. Ohno, T. Mitsui, M. Matsumura, Chem. Lett. 32 (2003) 364–365.
[9] Q. Xiao, L. Ouyang, J. Phys. Chem. Solids 72 (2011) 39–44.
[10] J.C. Colmenares, A. Magdziarz, D. Łomot, O. Chernyayeva, D. Lisovytskiy, Appl. Catal. B: Environ. 147 (2014) 624–632.
[11] C. Li, X. Yang, R. Chen, J. Pan, H. Tian, H. Zhu, X. Wang, A. Hagfeldt, L. Sun, Sol. Energy Mater. Sol. Cells 91 (2007) 1863–1871.
[12] R.L. Pozzo, M.A. Baltanás, A.E. Cassano, Catal. Today 39 (1997) 219–231.
[13] C. Águia, J. Ângelo, L.M. Madeira, A. Mendes, J. Environ. Manage. 92 (2011) 1724–1732.
[14] D.C. Hurum, A.G. Agrios, K.A. Gray, T. Rajh, M.C. Thurnauer, J. Phys. Chem. B 107 (2003) 4545–4549.
[15] R.I. Bickley, T. Gonzalez-Carreno, J.S. Lees, L. Palmisano, R.J.D. Tilley, J. Solid State Chem. 92 (1991) 178–190.
[16] A.G. Agrios, K.A. Gray, E. Weitz, Langmuir 20 (2004) 5911–5917.
[17] D.C. Hurum, K.A. Gray, T. Rajh, M.C. Thurnauer, J. Phys. Chem. B 108 (2004) 16483–16487.
[18] M. Hajaghazadeh, V. Vaiano, D. Sannino, H. Kakooei, R. Sotudeh-Gharebagh, P. Ciambelli, Catal. Today 230 (2014) 79–84.
[19] J. Taranto, D. Frochot, P. Pichat, Ind. Eng. Chem. Res. 48 (2009) 6229–6236.
[20] Y. Paz, in: I.d.L. Hugo, R. Benito Serrano (Eds.), Advances in Chemical Engineering Photocatalytic Technologies, Academic Press, 2009, pp. 289–336.
[21] M. Lewandowski, D.F. Ollis, Appl. Catal. B: Environ. 43 (2003) 309–327.
[22] C. Águia, J. Ângelo, L.M. Madeira, A. Mendes, Catal. Today 151 (2010) 77–83.
[23] L.A. Dibble, G.B. Raupp, Environ. Sci. Technol. 26 (1992) 492–495.
[24] J. Araña, A. Peña Alonso, J.M. Doña Rodríguez, J.A. Herrera Melián, O. González Díaz, J. Pérez Peña, Appl. Catal. B: Environ. 78 (2008) 355–363.
[25] Y. Yamin, N. Keller, V. Keller, J. Photochem. Photobiol. A 245 (2012) 43–57.
[26] R. Portela, S. Suárez, R.F. Tessinari, M.D. Hernández-Alonso, M.C. Canela, B. Sánchez, Appl. Catal. B: Environ. 105 (2011) 95–102.
[27] G.B. Raupp, A. Alexiadis, M.M. Hossain, R. Changrani, Catal. Today 69 (2001) 41–49.
[28] A.N. Kouamé, R. Masson, D. Robert, N. Keller, V. Keller, Catal. Today 209 (2013) 13–20.
[29] R.E. Hayes, S.T. Kolaczkowski, W.J. Thomas, Comput. Chem. Eng. 16 (1992) 645–657.
[30] S.A. Larson, J.A. Widegren, J.L. Falconer, J. Catal. 157 (1995) 611–625.

[31] T.H. Lim, S.D. Kim, Chemosphere 54 (2004) 305–312.
[32] F.V.S. Lopes, S.M. Miranda, R.A.R. Monteiro, S.D.S. Martins, A.M.T. Silva, J.L. Faria, R.A.R. Boaventura, V.J.P. Vilar, Appl. Catal. B: Environ. 140–141 (2013) 444–456.
[33] F.V.S. Lopes, R.A.R. Monteiro, A.M.T. Silva, G.V. Silva, J.L. Faria, A.M. Mendes, V.J.P. Vilar, R.A.R. Boaventura, Chem. Eng. J. 204–206 (2012) 244–257.
[34] M. Hussain, N. Russo, G. Saracco, Chem. Eng. J. 166 (2011) 138–149.
[35] Z. Pengyi, L. Fuyan, Y. Gang, C. Qing, Z. Wanpeng, J. Photochem. Photobiol. A 156 (2003) 189–194.
[36] S.M. Miranda, F.V.S. Lopes, C. Rodrigues-Silva, S.D.S. Martins, A.M.T. Silva, J.L. Faria, R.A.R. Boaventura, V.J.P. Vilar, Environ. Sci. Pollut. Res. (2014) 1–13.
[37] R.A.R. Monteiro, F.V.S. Lopes, A.M.T. Silva, J. Ângelo, G.V. Silva, A.M. Mendes, R.A.R. Boaventura, V.J.P. Vilar, Appl. Catal. B: Environ. 147 (2014) 988–999.
[38] T. Ohno, K. Sarukawa, K. Tokieda, M. Matsumura, J. Catal. 203 (2001) 82–86.
[39] B. Sun, A.V. Vorontsov, P.G. Smirniotis, Langmuir 19 (2003) 3151–3156.
[40] T. Ohno, K. Tokieda, S. Higashida, M. Matsumura, Appl. Catal. A: Gen. 244 (2003) 383–391.
[41] S. Sankar, K.G. Gopchandran, P. Kuppusami, S. Murugesan, Ceram. Int. 37 (2011) 3307–3315.
[42] X. Wang, L. Sø, R. Su, S. Wendt, P. Hald, A. Mamakhel, C. Yang, Y. Huang, B.B. Iversen, F. Besenbacher, J. Catal. 310 (2014) 100–108.
[43] V. Puddu, H. Choi, D.D. Dionysiou, G.L. Puma, Appl. Catal. B: Environ. 94 (2010) 211–218.
[44] M. Hussain, R. Ceccarelli, D.L. Marchisio, D. Fino, N. Russo, F. Geobaldo, Chem. Eng. J. 157 (2010) 45–51.
[45] J.M. Nicovich, S. Wang, M.L. McKee, P.H. Wine, J. Phys. Chem. 100 (1996) 680–688.
[46] N. Petit, A. Bouzaza, D. Wolbert, P. Petit, J. Dussaud, Catal. Today 124 (2007) 266–272.
[47] L.P. Thüner, I. Barnes, K.H. Becker, T.J. Wallington, L.K. Christensen, J.J. Orlando, B. Ramacher, J. Phys. Chem. A 103 (1999) 8657–8663.
[48] S. Yamazaki, H. Tsukamoto, K. Araki, T. Tanimura, I. Tejedor-Tejedor, M.A. Anderson, Appl. Catal. B: Environ. 33 (2001) 109–117.
[49] T.N. Obee, R.T. Brown, Environ. Sci. Technol. 29 (1995) 1223–1231.
[50] L. Cao, A. Huang, F.-J. Spiess, S.L. Suib, J. Catal. 188 (1999) 48–57.
[51] W.K. Jo, K.H. Park, Chemosphere 57 (2004) 555–565.
[52] J. Zhao, X. Yang, Build. Environ. 38 (2003) 645–654.
[53] P. Zhang, J. Liu, J. Photochem. Photobiol. A 167 (2004) 87–94.
[54] D.S. Muggli, J.L. Falconer, J. Catal. 191 (2000) 318–325.
[55] D.S. Muggli, J.L. Falconer, J. Catal. 187 (1999) 230–237.
[56] D.S. Muggli, S.A. Keyser, J.L. Falconer, Catal. Lett. 55 (1998) 129–135.
[57] M. El-Maazawi, A.N. Finken, A.B. Nair, V.H. Grassian, J. Catal. 191 (2000) 138–146.
[58] T. Ohno, K. Sarukawa, M. Matsumura, J. Phys. Chem. B 105 (2001) 2417–2420.
[59] A. Hagfeldt, M. Graetzel, Chem. Rev. 95 (1995) 49–68.
[60] S. Yamazaki, T. Tanimura, A. Yoshida, K. Hori, J. Phys. Chem. A 108 (2004) 5183–5188.
[61] G. Lu, A. Linsebigler, J.T. Yates, J. Phys. Chem. 99 (1995) 7626–7631.
[62] J. Fan, J.T. Yates, J. Am. Chem. Soc. 118 (1996) 4686–4692.
[63] J. Ângelo, L. Andrade, A. Mendes, Manuscript submitted for publication (2014).
[64] R.A.R. Monteiro, S.M. Miranda, V.J.P. Vilar, L.M. Pastrana-Martínez, P.B. Tavares, R.A.R. Boaventura, J.L. Faria, E. Pinto, A.M.T. Silva, Appl. Catal. B: Environ. 162 (2015) 66–74.